Journal of Magnetism and Magnetic Materials 397 (2016) 233–239

Contents lists available at ScienceDirect

Journal of Magnetism and Magnetic Materials

journal homepage: www.elsevier.com/locate/jmmm

Mechanically induced magnetic diffusion in cylindrical magnetoelastic materials

Justin J. Scheidler, Marcelo J. Dapino *

Department of Mechanical and Aerospace Engineering, The Ohio State University, 201 W. 19th Ave., Columbus, OH 43210, USA

ARTICLE INFO

Article history:
Received 29 April 2015
Received in revised form
5 August 2015
Accepted 19 August 2015
Available online 22 August 2015

Keywords:
Magnetic diffusion
Eddy currents
Magnetostrictive materials
Ferromagnetic shape memory alloys
Dynamic stress
Dynamic strain

ABSTRACT

This paper considers the radial dependence of magnetic diffusion in cylindrical magnetoelastic materials that results from the simultaneous application of a constant surface magnetic field and a dynamic mechanical input. Mechanically induced magnetic diffusion is particularly pronounced in materials that exhibit a strong magnetoelastic coupling, such as magnetostrictive materials and ferromagnetic shape memory alloys. Analytical time- and frequency-domain solutions of the PDE governing the radial diffusion of magnetic field are derived. The solutions are non-dimensionalized by deriving a skin depth and cut-off frequency for mechanically induced diffusion, which are about 2.08 and 4.34 times those for field-induced diffusion, respectively. It is shown that the effects of mechanically induced diffusion can be incorporated in linear constitutive models through the use of a complex-valued, frequency-dependent magnetoelastic coupling coefficient and Young's modulus. The solutions show that for forcing frequencies f up to about the cut-off frequency, the magnitude of the steady-state, dynamic field increases in proportion to f. As forcing frequency increases above that range, the magnitude overshoots its high frequency limit, peaks, then decreases to its high frequency limit, at which point the dynamic magnetic flux becomes zero and continued increases in forcing frequency have no effect. Together, the derived frequency responses, skin depth, and cut-off frequency can be used to design magnetoelastic systems and determine if lamination of the magnetoelastic material is necessary

1. Introduction

Eddy currents inside electrically conducting media alter the propagation of magnetic fields into the media; the resulting attenuation and phase lag of the magnetic fields is quantified by magnetic diffusion laws. Magnetic diffusion in ferromagnets caused by the application of dynamic magnetic fields is a classical problem that has received significant attention since the late 1800s [1–3]. The influence of magnetoelasticity and static stress on field-induced magnetic diffusion has been investigated only more recently [4–6].

Dynamic mechanical inputs cause a diffusion of static magnetic fields into electrically conducting magnetoelastic materials, particularly ones that exhibit strong coupling, such as magnetostrictive materials and ferromagnetic shape memory alloys. Mechanically induced magnetic diffusion is critically important for applications in which these materials operate under dynamic mechanical loading, including dynamic sensors, energy harvesters, vibration dampers, and stiffness tuning devices. However, only a few studies on this effect have been reported.

The effects of 1D mechanically induced magnetic diffusion have been briefly studied numerically [7–9]. Sarawate and Dapino [7] investigated the magnetic field in a Ni–Mn–Ga rod and illustrated the dependence of the field's time-domain response on the radial coordinate and strain frequency for a small range of parameters. 1D mechanically induced magnetic diffusion has been analytically treated in the context of magnetostrictive energy harvesters by Davino et al. [10], who derived an expression for average harvested power, and by Zhao and Lord [11], who derived an expression for the effective internal magnetic field. However, the spatial and frequency dependence of the internal magnetic field or magnetic flux density have not been derived. Further, calculation of a skin depth and cut-off frequency for this effect are absent from the literature.

This paper presents an analytical model of linear, 1D mechanically induced magnetic diffusion in cylindrical magnetoelastic materials. The model is used to quantify the radial dependence of internal magnetic fields created by eddy currents that result from the application of harmonic, axial stresses. Analytical time- and frequency-domain solutions are derived for a constant, axial surface magnetic field after considering the axial symmetry and assuming (i) negligible displacement currents, (ii) linear

* Corresponding author.
E-mail address: dapino.1@osu.edu (M.J. Dapino).

http://dx.doi.org/10.1016/j.jmmm.2015.08.074
0304-8853/

constitutive behavior, (iii) negligible demagnetizing fields, and (iv) uniform stress and electrical conductivity . The solutions are non-dimensionalized and then used to investigate the spatial and frequency dependence of the internal magnetic field and magnetic flux. Unlike the referenced analytical and numerical solutions, these analytical solutions provide design criteria, reveal the relative importance of each material property, and provide expressions for skin depth and cut-off frequency. For nonlinear operating regimes, the derived solutions can be used to assess whether lamination of the magnetoelastic material is necessary.

2. Model development

The general magnetic diffusion equation for magnetoelastic materials is derived from Maxwell's equations and the assumption that displacement currents are negligible

$$-\nabla\left(\nabla\cdot\vec{H}\right)+\nabla^2\vec{H}=\sigma\vec{B}_t=\sigma\mu_0\left(\vec{H}+\vec{M}\right)_t, \tag{1}$$

where the subscript t denotes partial differentiation with respect to time, σ represents the electrical conductivity, μ_0 is the magnetic permeability of free space, and $\vec{H}$, $\vec{B}$, and $\vec{M}$ are the magnetic field strength, magnetic flux density, and magnetization vectors, respectively, which each depend on time t and position. In magnetostrictive materials, $\vec{M}$ depends on the stress vector $\vec{T}$ such that (1) becomes

$$-\nabla\left(\nabla\cdot\vec{H}\right)+\nabla^2\vec{H}-\sigma\left(\left[\mu\right]\vec{H}\right)_t=\sigma\left(\left[d^*\right]\vec{T}\right)_t, \tag{2}$$

where $[\mu]$ and $[d^*]$ denote the magnetic field- and stress-dependent magnetic permeability and piezomagnetic coefficient tensors, respectively. In ferromagnetic shape memory alloys, $\vec{M}$ depends on the strain vector $\vec{S}$ such that (1) becomes

$$-\nabla\left(\nabla\cdot\vec{H}\right)+\nabla^2\vec{H}-\sigma\left(\left[\mu\right]\vec{H}\right)_t=\sigma\left(\mu_0\left[e\right]\vec{S}\right)_t, \tag{3}$$

where $[e]$ represents the magnetic field- and strain-dependent coupling coefficient tensor.

For biased operation and sufficiently low amplitude excitation, the constitutive tensors $[\mu]$, $[d^*]$, and $[e]$ can be assumed to be constant. If a cylindrical magnetostrictive material or ferromagnetic shape memory alloy is operated in a transducer having a closed magnetic circuit of low reluctance, demagnetizing fields can be neglected and the circuit can be represented as an infinitely long rod subjected to a uniform, axial magnetic field H_{ext} at its surface and an axial, distributed force on its ends. Due to the inhomogeneous internal magnetic field, the rod's stiffness, and therefore the applied stress, will be radially dependent [4]. However, to permit an analytical solution, the stress is assumed to be uniform throughout the rod. Stress uniformity along the axial direction is valid for forcing frequencies sufficiently below mechanical resonance of the rod. Due to this assumption, the rod's mechanical inertia and damping (i.e., structural dynamics) are ignored.

Under the aforementioned assumptions, (2) and (3) simplify to

$$H_{rr}(r,t)+H_r(r,t)/r-\sigma\mu H_t(r,t)=\sigma d^* T_t(t), \tag{4}$$

and

$$H_{rr}(r,t)+H_r(r,t)/r-\sigma\mu H_t(r,t)=\sigma\mu_0 e S_t(t), \tag{5}$$

respectively, where r is the radial coordinate, the subscript r denotes partial differentiation with respect to r, and μ, d^*, and e are the 33 components of the respective tensors. Thus, the 1D magnetic diffusion problem for ferromagnetic shape memory alloys is identical to that for magnetostrictive materials if $\mu_0 e$ and $S(t)$ are substituted for d^* and $T(t)$, respectively. Consequently, it is sufficient to only solve (4), which resembles the 1D field-induced magnetic diffusion problem, but with a forcing term. Fig. 1 depicts the general mechanically induced magnetic diffusion problem for axial loading of a magnetoelastic cylinder and the simplified problem that is solved.

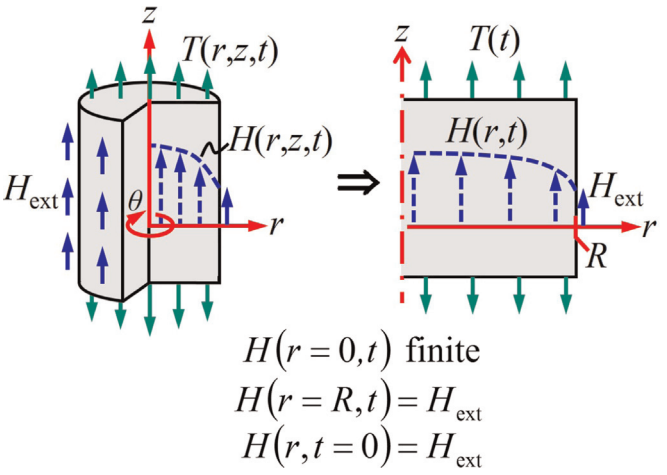

Fig. 1. General mechanically induced magnetic diffusion problem for axial loading (left) and the simplified 1D problem that is solved (right); the magnetic field at the surface of the rod, H_{ext}, is assumed to be uniform and constant in time.

3. 1D time- and frequency-domain solutions

To solve (4), it is convenient to have zero boundary conditions. This is accomplished using the change of variables $\tilde{H}(r,t)=H(r,t)-H_{\text{ext}}$, so that the initial boundary value problem is written as

$$\tilde{H}_{rr}(r,t)+\tilde{H}_r(r,t)/r-\sigma\mu\tilde{H}_t(r,t)=\sigma d^* T_t(t), \tag{6}$$

$$\tilde{H}(r,t=0)=0, \tag{7}$$

$$\tilde{H}(r=R,t)=0, \tag{8}$$

$$\tilde{H}(r=0,t)\ \text{finite}, \tag{9}$$

where $r=R$ is the surface of the rod. Eqs. (6)–(9) can be written as an inhomogeneous Bessel equation of order zero using the change of variables, $u=\sqrt{\mu\sigma}r$,

$$u^2\tilde{H}_{uu}(u,t)+u\tilde{H}_u(u,t)-u^2\tilde{H}_t(u,t)=\frac{d^*}{\mu}u^2T_t(t), \tag{10}$$

$$\tilde{H}\left(\frac{u}{\sqrt{\mu\sigma}},t=0\right)=0, \tag{11}$$

$$\tilde{H}\left(u=\sqrt{\mu\sigma}R,t\right)=0, \tag{12}$$

$$\tilde{H}(u=0,t)\ \text{finite}, \tag{13}$$

where the subscript u indicates partial differentiation with respect to u.

The solution of (10)–(13) is found using the method of eigenfunction expansions. After assuming that $\tilde{H}(u, t) = D(t)U(u)$, the eigenvalue problem can be derived from the homogeneous form of (10) using the method of separation of variables

$$u^2U_{uu}(u) + uU_u(u) = ku^2U(u), \tag{14}$$

$$U(0) \text{ finite}, \tag{15}$$

$$U\left(\sqrt{\mu\sigma}R\right) = 0, \tag{16}$$

where the separation constant k must be negative (i.e., $k = -\lambda^2$) to avoid trivial solutions [12]. The solution of the eigenvalue problem (14)–(16) is given by Asmar [12] as

$$U^n(u) = J_0\left(\frac{\alpha_0^n}{\sqrt{\mu\sigma}R}u\right), \tag{17}$$

corresponding to the eigenvalues

$$\left(\lambda^n\right)^2 = \left(\alpha_0^n/\left(\sqrt{\mu\sigma}R\right)\right)^2, \tag{18}$$

where $n = 1, 2, 3\ldots$ is an index, J_0 is the Bessel function of order zero, and α_0^n is the nth positive zero of J_0. Using the method of eigenfunction expansions, the solution of (10) has the form

$$\tilde{H}(u, t) = \sum_{n=1}^{\infty} D^n(t)U^n(u) = \sum_{n=1}^{\infty} D^n(t)J_0\left(\frac{\alpha_0^n}{\sqrt{\mu\sigma}R}u\right). \tag{19}$$

Insertion of (19) into (10) followed by simplification using (14) and (17) gives

$$\sum_{n=1}^{\infty}\left[J_0\left(\frac{\alpha_0^n}{\sqrt{\mu\sigma}R}u\right)\left(D_t^n(t) + \left(\lambda^n\right)^2D^n(t)\right)\right] = -\frac{d^*T_t(t)}{\mu}. \tag{20}$$

After multiplying both sides of (20) by $uJ_0(\alpha_0^s u/(\sqrt{\mu\sigma}R))$, integrating with respect to u from 0 to $\sqrt{\mu\sigma}R$, interchanging the order of integration and summation, and using the orthogonality of the Bessel functions [12], only the sth term of the summation survives

$$\frac{\mu\sigma R^2}{2}J_1^2(\alpha_0^s)\left(D_t^s(t) + \left(\lambda^s\right)^2D^s(t)\right) = -\frac{d^*}{\mu}T_t(t)\int_0^{\sqrt{\mu\sigma}R} uJ_0\left(\frac{\alpha_0^s}{\sqrt{\mu\sigma}R}u\right)du, \tag{21}$$

where J_1 is the Bessel function of order 1. Evaluating the integral in (21) using the change of variables, $k = \alpha_0^s u/(\sqrt{\mu\sigma}R)$, and an integral identity of Bessel functions [12], one gets

$$D_t^s(t) + \left(\lambda^s\right)^2D^s(t) = -\frac{2d^*}{\mu\alpha_0^sJ_1(\alpha_0^s)}T_t(t), \tag{22}$$

$$D^s(0) = 0. \tag{23}$$

The initial condition (23) is derived by inserting (19) into (11) to get

$$\tilde{H}(r, t = 0) = \sum_{s=1}^{\infty} D^s(0)J_0\left(\frac{\alpha_0^s}{R}r\right) = 0, \tag{24}$$

which is a 0th order Bessel series expansion of $f(r) = 0$, for which the expansion coefficients $D^s(0)$ must all equal zero. For a harmonic stress, $T(t) = \hat{T}\exp(j\omega t)$, the solution of (22)–(23) is

$$D^s(t) = \hat{T}M^s(\omega)\left(e^{j(\omega t+\phi^s(\omega))} - e^{j\phi^s(\omega)}e^{-\left(\lambda^s\right)^2t}\right), \tag{25}$$

where the magnitude $M^s(\omega)$ and phase $\phi^s(\omega)$ of the modal frequency response $\hat{D}^s(j\omega)$ are

$$M^s(\omega) = \left(\left(\hat{D}_{\text{Re}}^{\ s}(\omega)\right)^2 + \left(\hat{D}_{\text{Im}}^{\ s}(\omega)\right)^2\right)^{1/2} \tag{26}$$

and

$$\phi^s(\omega) = \angle\left(\hat{D}_{\text{Re}}^{\ s}(\omega) + j\hat{D}_{\text{Im}}^{\ s}(\omega)\right), \tag{27}$$

where

$$\hat{D}_{\text{Re}}^{\ s}(\omega) = \frac{-2d^*\left(\mu\sigma\omega R^2\right)^2}{\mu\alpha_0^sJ_1\left(\alpha_0^s\right)\left(\left(\alpha_0^s\right)^4 + \left(\mu\sigma\omega R^2\right)^2\right)}, \tag{28}$$

$$\hat{D}_{\text{Im}}^{\ s}(\omega) = \frac{-2d^*\alpha_0^s\left(\mu\sigma\omega R^2\right)}{\mu J_1\left(\alpha_0^s\right)\left(\left(\alpha_0^s\right)^4 + \left(\mu\sigma\omega R^2\right)^2\right)}. \tag{29}$$

The total time-domain solution in the original coordinates is

$$H(r, t) = \sum_{s=1}^{\infty}\left[D^s(t)J_0\left(\alpha_0^s\frac{r}{R}\right)\right] + H_{\text{ext}}, \tag{30}$$

where the real and the imaginary part of (25) are retained for cosinusoidal and sinusoidal forcing, respectively. By inserting the steady-state part of (25) into (19), the frequency response of $\tilde{H}(r, t)$ can be written as

$$G(r, j\omega) = \hat{T}\sqrt{G_{\text{Re}}^2 + G_{\text{Im}}^2}\ \exp\left(j\angle\left(G_{\text{Re}} + jG_{\text{Im}}\right)\right), \tag{31}$$

where

$$G_{\text{Re}}(r, \omega) = \sum_{s=1}^{\infty}\left[J_0\left(\alpha_0^s\frac{r}{R}\right)\hat{D}_{\text{Re}}^{\ s}(\omega)\right], \tag{32}$$

$$G_{\text{Im}}(r, \omega) = \sum_{s=1}^{\infty}\left[J_0\left(\alpha_0^s\frac{r}{R}\right)\hat{D}_{\text{Im}}^{\ s}(\omega)\right]. \tag{33}$$

4. Non-dimensionalization of the analytical solutions

The time-domain solution is non-dimensionalized in two steps. First, the rod's radius is written in terms of a parameter q and penetration (skin) depth δ as

$$\frac{R}{\delta} = q. \tag{34}$$

For field- and mechanically induced diffusion, the skin depth can be generally defined as the depth from the surface at which the amplitude of the dynamic magnetic flux $\tilde{B}$ has attenuated by an amount ψ relative to the amplitude at the surface. Using the linear piezomagnetic equation

$$\tilde{B}(r, t) = \mu\tilde{H}(r, t) + d^*T(t) \tag{35}$$

and boundary condition (8), the surface field is $\tilde{B}(r = R, t) = d^*T(t)$. Consequently, if $R = \delta$ then

$$\left|\tilde{B}(r = 0, t)\right| = \psi\left|\tilde{B}(r = R, t)\right| = \psi d^*\hat{T}. \tag{36}$$

Evaluation of (36) using (35) and the steady-state response of (19) followed by simplification gives

$$\left|\sum_{s=1}^{\infty}\left[\frac{\left(-2p^2/\alpha_0^s\right) + j\left(-2p\alpha_0^s\right)}{J_1\left(\alpha_0^s\right)\left(\left(\alpha_0^s\right)^4 + p^2\right)}\right] + 1\right| = \psi, \tag{37}$$

where $p = \mu\sigma\omega\delta^2$. For field-induced diffusion of plane waves, $\psi = \exp(-1)$ [1], whereas for field-induced diffusion in cylinders, $\psi = (J_0(\sqrt{-1}))^{-1}$ [13]. By numerically solving (37) for the latter condition, one gets $p \approx 4.3393$. Thus, the skin depth for mechanically induced diffusion in cylinders is

$$\delta^M \approx 2.0831(\mu\sigma\omega)^{-1/2} = 2.0831\delta^H, \tag{38}$$

where δ^H is the skin depth for field-induced diffusion in cylinders, which is given in [13]. The condition $\delta^M = \delta^H$ can be specified, but at the expense of having a different meaning (i.e., different ψ) for the skin depth for the two types of diffusion. Thus, δ^M as given by (38) is used in this paper.

The second step used to non-dimensionalize the time-domain solution is to non-dimensionalize the dynamic field such that the dynamic flux it would produce on its own is normalized by the magnitude of the dynamic flux produced by the stress alone. Therefore, the non-dimensionalized dynamic field is

$$\bar{H}(r, t) = \frac{\mu}{\left|d^*\hat{T}\right|}\tilde{H}(r, t), \tag{39}$$

while the non-dimensionalized total field is $\acute{H}(r, t) = \bar{H}(r, t) + H_{\text{ext}}$.

To non-dimensionalize the frequency-domain solution, the first step is to normalize the frequency by a cut-off frequency defined as the frequency for which $\delta = R$ [13]. Using (38), the cut-off frequency for mechanically induced diffusion is given as

$$\omega_c^M \approx \left(2.0831\right)^2\left(\mu\sigma R^2\right)^{-1} = 4.3393\omega_c^H, \tag{40}$$

where ω_c^H is the cut-off frequency for field-induced diffusion in cylinders, which is given in [13]. Thus, by comparing (40) to (34) and (38), it is found that the frequency can be scaled according to

$$\omega = q^2\omega_c^M. \tag{41}$$

The second non-dimensionalization step is the same as that used for the time-domain solution (i.e., (39)).

The non-dimensionalized time-domain solution is given as follows. The use of (34) and (38) in (39) followed by simplification gives

$$\bar{H}\left(\frac{r}{R}, t\right) = \sum_{s=1}^{\infty}\left[J_0\left(\alpha_0^s\frac{r}{R}\right)\bar{M}^s\left(q\right)\left(W(t) - X(t)\right)\right], \tag{42}$$

where

$$W(t) = \exp\left(j\left(\omega t + \bar{\phi}^s(q)\right)\right), \tag{43}$$

$$X(t) = \exp(j\bar{\phi}^s(q))\exp\left(-\frac{(\alpha_0^s)^2\omega}{4.3393q^2}t\right). \tag{44}$$

As before, the real and imaginary parts of (43) and (44) are retained for cosinusoidal and sinusoidal forcing, respectively. The magnitude $\bar{M}^s(q)$ and phase $\bar{\phi}^s(q)$ of $\bar{D}^s(jq)$ are calculated analogous to (26) and (27), where the real and imaginary parts of $\bar{D}^s(jq)$ are, respectively,

$$\bar{D}_{\text{Re}}^s(q) = \frac{-2\,\text{sgn}\left(d^*\hat{T}\right)\left(4.3393q^2\right)^2}{\alpha_0^s J_1\left(\alpha_0^s\right)\left(\left(\alpha_0^s\right)^4 + \left(4.3393q^2\right)^2\right)} \tag{45}$$

and

$$\bar{D}_{\text{Im}}^s(q) = \frac{-2\,\text{sgn}\left(d^*\hat{T}\right)\alpha_0^s\left(4.3393q^2\right)}{J_1\left(\alpha_0^s\right)\left(\left(\alpha_0^s\right)^4 + \left(4.3393q^2\right)^2\right)}, \tag{46}$$

where sgn() is the signum function. The magnitude of the steady-state, non-dimensionalized dynamic field

$$\left|\bar{H}\left(\frac{r}{R}, t\to\infty\right)\right| = \sum_{s=1}^{\infty}\left[J_0\left(\alpha_0^s\frac{r}{R}\right)\sqrt{\left(\bar{D}_{\text{Re}}^s\right)^2 + \left(\bar{D}_{\text{Im}}^s\right)^2}\right], \tag{47}$$

is only a function of r/R and q.

The frequency response of $\bar{H}(r/R, t)$ is

$$\bar{G}\left(\frac{r}{R}, jq\right) = \frac{\mu}{\left|d^*\hat{T}\right|}G\left(r, j\left(q^2\omega_c^M\right)\right)$$

$$= \sqrt{\bar{G}_{\text{Re}}^2 + \bar{G}_{\text{Im}}^2}\,\exp\left(j\angle\left(\bar{G}_{\text{Re}} + j\bar{G}_{\text{Im}}\right)\right), \tag{48}$$

where

$$\bar{G}_{\text{Re}}\left(\frac{r}{R}, q\right) = \sum_{s=1}^{\infty}\left[J_0\left(\alpha_0^s\frac{r}{R}\right)\bar{D}_{\text{Re}}^s\left(q\right)\right], \tag{49}$$

$$\bar{G}_{\text{Im}}\left(\frac{r}{R}, q\right) = \sum_{s=1}^{\infty}\left[J_0\left(\alpha_0^s\frac{r}{R}\right)\bar{D}_{\text{Im}}^s\left(q\right)\right]. \tag{50}$$

A non-dimensionalized magnetic flux density can be defined as the dynamic flux density normalized by its magnitude at the surface

$$\bar{B}\left(\frac{r}{R}, t\right) = \frac{\tilde{B}(r, t)}{\left|d^*\hat{T}\right|}. \tag{51}$$

After inserting (35) and (19) into (51) and simplifying, the frequency response of $\bar{B}(r/R, t)$ can be expressed as

$$\bar{F}\left(\frac{r}{R}, jq\right) = \left(\bar{G}_{\text{Re}} + \text{sgn}\left(d^*\hat{T}\right)\right) + j\,\bar{G}_{\text{Im}}. \tag{52}$$

5. Eddy current effects in 0D constitutive models

To incorporate the effects of mechanically induced magnetic diffusion in 0D linear constitutive models, an effective internal magnetic field is first defined as the average field over the rod's cross section

$$H_{\text{eff}}(t) = \frac{1}{\pi R^2}\int_A H(r, t)\,dA = \frac{2}{R^2}\int_0^R H(r, t)r\,dr, \tag{53}$$

where A is the cross-sectional area. Inserting (30) into (53), neglecting the transient part of (25), evaluating the integral as done in (21), and simplifying, one gets

$$H_{\text{eff}}(t) = 2\sum_{s=1}^{\infty}\left[\frac{\hat{D}^s(j\omega)J_1\left(\alpha_0^s\right)}{\alpha_0^s}\right]\hat{T}e^{j\omega t} + H_{\text{ext}} = \hat{H}_{\text{eff}}T(t) + H_{\text{ext}}. \tag{54}$$

The use of the effective field (54) in the 0D linear piezomagnetic equation $B(t) = \mu H(t) + d^*T(t)$ results in

$$B(t) = \mu H_{\text{ext}} + \left(d^* + \mu\hat{H}_{\text{eff}}\right)T(t) = \mu H_{\text{ext}} + d^*\chi^M T(t). \tag{55}$$

$\chi^M = \chi_{\text{Re}}^M - j\,\chi_{\text{Im}}^M$ is the eddy current loss factor for mechanically induced diffusion

$$\chi_{\text{Re}}^M = 1 - 4\sum_{s=1}^{\infty}\left[\frac{\left(4.3393q^2\right)^2}{\left(\alpha_0^s\right)^2\left(\left(\alpha_0^s\right)^4 + \left(4.3393q^2\right)^2\right)}\right], \tag{56}$$

$$\chi_{\mathrm{Im}}^{M} = 4\sum_{s=1}^{\infty}\left[\frac{4.3393q^2}{(\alpha_0^s)^4 + (4.3393q^2)^2}\right], \tag{57}$$

where (41) and (40) were used to simplify the expressions. Consequently, mechanically induced magnetic diffusion effects can be represented in linear models of magnetostrictive materials as a complex-valued, frequency-dependent piezomagnetic coefficient (or, in general, as a complex-valued, frequency-dependent coupling coefficient in magnetoelastic materials)

$$d_c^* = d^*\chi^M = d^*\left(\chi_{\mathrm{Re}}^{M} - j\,\chi_{\mathrm{Im}}^{M}\right). \tag{58}$$

This is analogous to the representation of field-induced diffusion as a complex-valued magnetic permeability [13]. The non-dimensionalized, effective dynamic field can now be written as

$$\bar{H}_{\mathrm{eff}}(t) = \mathrm{sgn}\left(d^*\hat{T}\right)\left(\left(\chi_{\mathrm{Re}}^{M} - 1\right) - j\chi_{\mathrm{Im}}^{M}\right)\mathrm{e}^{j\omega t}. \tag{59}$$

If the effective field (54) is instead inserted into the 0D linear piezomagnetic equation $S(t) = dH(t) + T(t)/E$, the following results:

$$\begin{aligned} S(t) &= dH_{\mathrm{ext}} + \left(\frac{1}{E} + d\hat{H}_{\mathrm{eff}}\right)T(t) \\ &= dH_{\mathrm{ext}} + \frac{1}{E}\left(1 + \left(\chi^M - 1\right)\frac{dd^*E}{\mu}\right)T(t) \\ &= dH_{\mathrm{ext}} + \frac{1}{E}\left(1 + \left(\chi^M - 1\right)\kappa^2\right)T(t), \end{aligned} \tag{60}$$

where E is Young's modulus, $d = d^*$, and κ is the magnetomechanical coupling factor. Thus, mechanically induced magnetic diffusion also causes the magnetoelastic material's modulus to be a complex-valued function of the excitation frequency

$$E_c = E\frac{1}{1 + \left(\chi^M - 1\right)\kappa^2}. \tag{61}$$

6. Results and discussion

The derived solutions involve infinite summations. For the cases considered in this paper, 20 terms are sufficient to ensure convergence of the summations; to generate the following figures, summations were truncated at 500 terms. The general solutions given in Sections 4 and 5 are illustrated below; thus, the following figures and discussion are valid for all magnetoelastic materials when their behavior is sufficiently linear.

The non-dimensionalized time-domain behavior of mechanically induced diffusion is shown in Fig. 2 for positive $d^*\hat{T}$. If $d^*\hat{T}$ is negative, the response is the negative of that shown in Fig. 2. The spatial dependence of $\bar{H}(r/R, t)$ is depicted in Fig. 2a for $R/\delta^M = q = 1$. The transient response quickly decays, and the internal magnetic field becomes nearly sinusoidal in time. The amplitude and the phase lag of the steady-state response increase while moving from the rod's surface to its axis. Fig. 2b shows the frequency dependence of the non-dimensionalized, effective dynamic field $\bar{H}_{\mathrm{eff}}(t)$ for different q. As q increases, the amplitude and the phase lag increase monotonically from 0 and $\pi/2$ to 1 and π, respectively. The prior numerical solutions [7,8] are consistent with these trends.

Physically, as the magnitude of the non-dimensionalized dynamic field increases from 0 toward 1, the magnetic energy increases in magnitude and varies with time such that it opposes changes in the magnetoelastic coupling energy. This suppresses changes in magnetization, leading to a reduction in magnetic flux

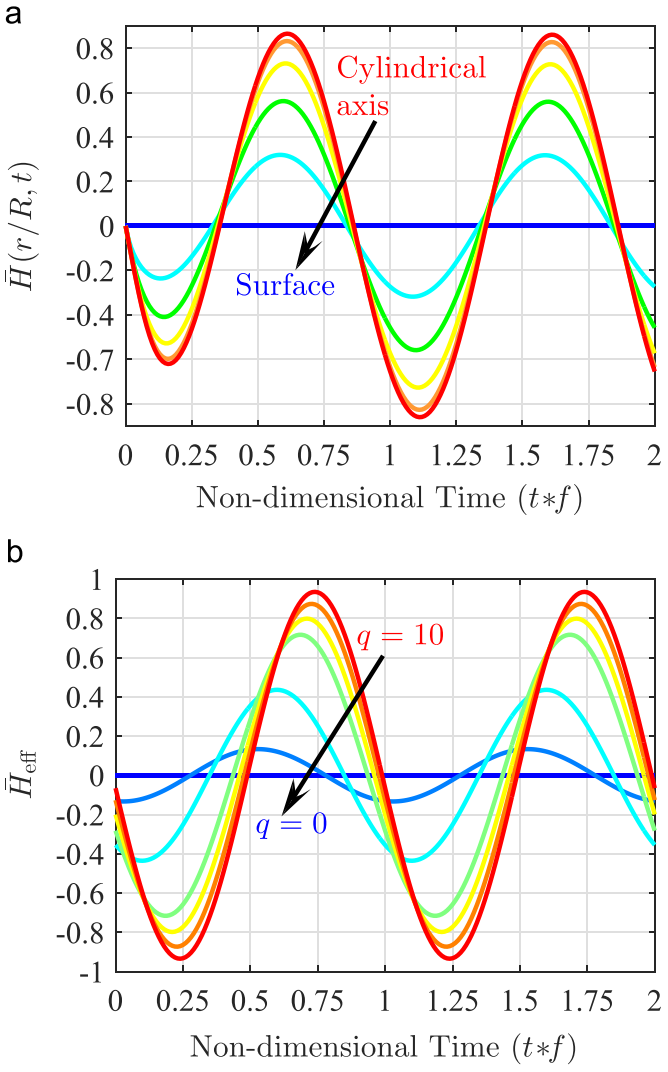

Fig. 2. Non-dimensionalized time-domain response to sinusoidal forcing for positive $d^*\hat{T}$, (a) non-dimensionalized dynamic field $\bar{H}(r/R, t)$ at radial locations of 0 (cylindrical axis), 0.2R, 0.4R, 0.6R, 0.8R, and 0.9R (distance from the axis increases from red to blue – the direction of the arrow) for $R/\delta^M = q = 1$ and (b) non-dimensionalized, effective dynamic field $\bar{H}_{\mathrm{eff}}(t)$ for $R/\delta^M = q$ of 0, 0.5, 1, 2, 3, 5, and 10 (q decreases from red to blue – the direction of the arrow). (For interpretation of the references to color in this figure legend, the reader is referred to the web version of this article.)

changes and a stiffening of the elastic behavior. When the non-dimensionalized dynamic field has a magnitude of 1 and lags behind the stress by π (or by 0 for a material with negative d^*), changes in the magnetoelastic coupling energy are balanced by changes in the magnetic energy. As a result, there is no driving potential to vary the magnetization from its bias value. Therefore, the magnetic flux remains constant and the material behaves passively. This state forms the upper bound on mechanically induced magnetic diffusion. From this state, increases in q will have no effect on the constitutive response at radial locations for which the upper bound has been reached.

Fig. 3 depicts the steady-state, spatial distribution of the magnitude of the non-dimensionalized dynamic field, which is only a function of $R/\delta^M = q$. In each case, the dynamic field is zero at the rod's surface due to the boundary condition (8). Thus, mechanically induced changes in magnetization are unimpeded at the surface, where the dynamic magnetic flux attains its maximum value. When the radius is one skin depth (i.e., $q=1$), the magnitude of the non-dimensionalized dynamic field at the rod's axis is

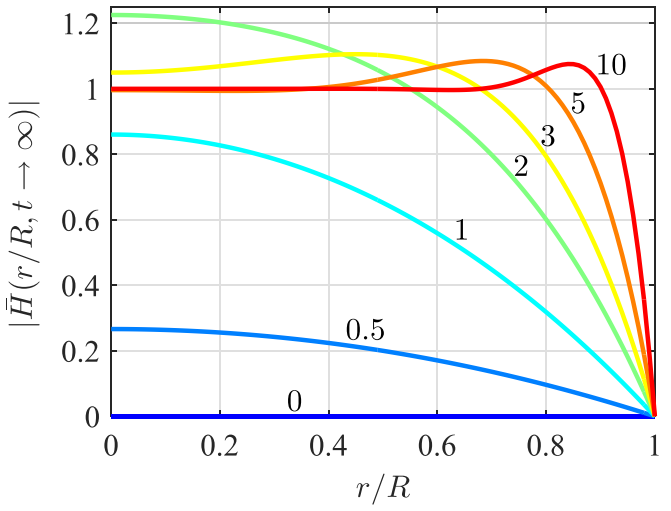

Fig. 3. Spatial distribution of the steady-state, non-dimensionalized dynamic field for different $R/\delta^M = q$.

about 0.86. As q increases, magnetic diffusion becomes more severe and the magnitude of the internal dynamic field increases accordingly. Interestingly, for moderate to high q, the magnitude of the non-dimensionalized dynamic field exceeds 1. This is discussed after presenting the frequency-domain responses.

The non-dimensionalized frequency response of $\bar{H}(r/R, t)$ at different radial locations is presented in Fig. 4a. For ω/ω_c less than about 1, the magnitude response increases monotonically with frequency and with decreasing r. In this regime, $|\bar{G}(r/R, jq)| \propto f^{1.0}$. With further increases in frequency, the magnitude overshoots 1, peaks, then decreases to 1 and becomes independent of frequency. The peak magnitude decreases and is successively shifted to higher frequencies as one moves closer to the rod's surface. The normalized, frequency-independent field magnitude is 1 at all locations. A $-\pi/2$ phase shift occurs as frequency increases. The response toward the surface leads that at the axis, particularly after the magnitude response at the axis peaks.

To explain the frequency response in Fig. 4a, recall that diffusion-produced fields are in phase with the eddy currents (Ampère's law), which are induced in proportion to $-B_t(t)$ (Faraday–Lenz law). Consequently, $\tilde{H}(r, t) \propto -B_t(r, t)$. At low frequency, the internal magnetic field is nearly constant and $-B_t(r, t) \approx -d{*}T_t(t)$; thus, the internal field is in phase with $-d{*}T_t(t)$, which lags $\pi/2$ behind $T(t)$. As frequency increases, the magnitude of the internal field increases along with the proportion of $-B_t(r, t)$ caused by the field. As a result, $B(r, t)$ phase shifts toward $\tilde{H}(r, t)$ and lags behind $T(t)$. This in turn creates a lag in the eddy currents and $\tilde{H}(r, t)$. This behavior continues with increasing frequency until $H(t)$ lags behind $T(t)$ by π, at which point the magnitude of $\tilde{H}(r, t)$ becomes frequency independent. The overshoot in the magnitude response of $\bar{H}(r/R, t)$ results from the non-180° phase misalignment between the dynamic field and the stress; it does not imply that the dynamic field overcomes the applied stress and begins to drive the system. To illustrate this, the magnitude response of the non-dimensionalized dynamic flux is shown in Fig. 4b. At the cut-off frequency, the magnitude of the non-dimensionalized dynamic flux is $0.789 \approx (J_0(\sqrt{-1}))^{-1}$ at the axis; thus, the derivation of the cut-off frequency in Section 4 is verified. Above the cut-off frequency, the magnitude decays monotonically to zero, first at the axis, then closer to the surface.

Given a maximum desired attenuation of the magnetic flux density, Fig. 4b can be used to define design criteria for applications in which cylindrical magnetoelastic materials are subjected to dynamic axial stress. In practice, the maximum allowable

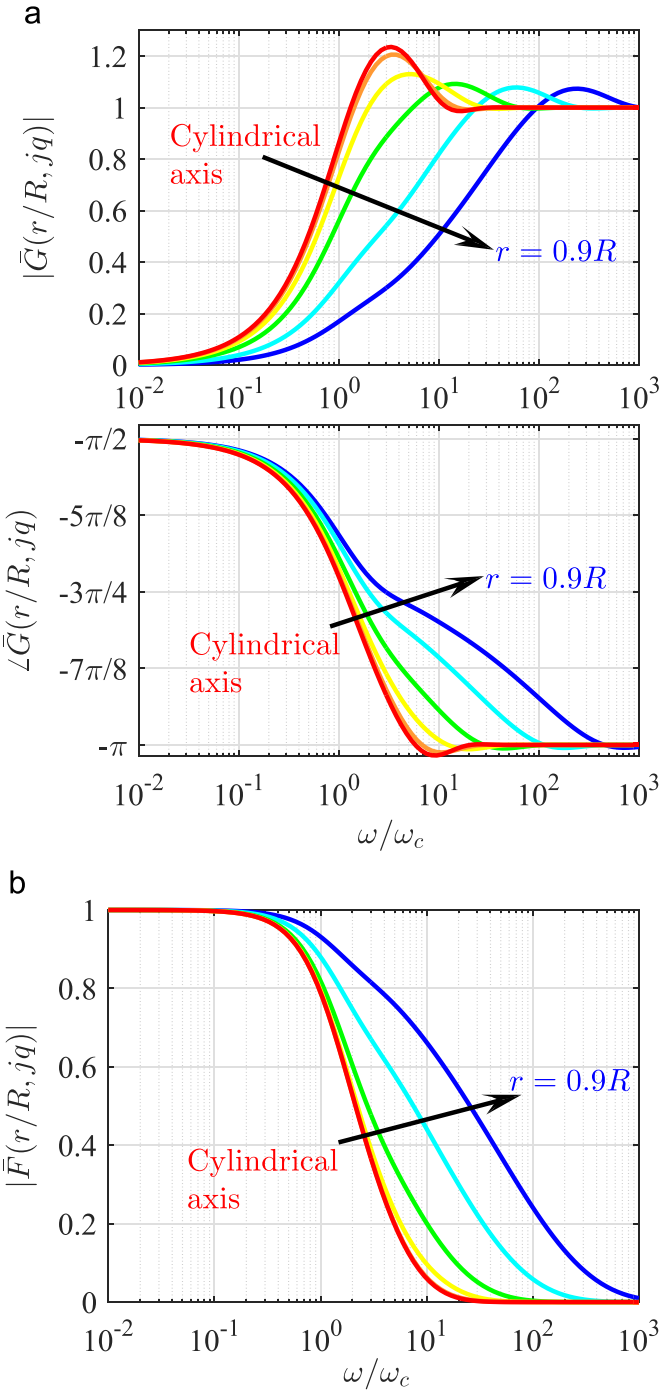

Fig. 4. Non-dimensionalized frequency response of (a) the dynamic field $\tilde{H}(r, t)$ – magnitude (top) and phase (bottom) – and (b) the dynamic magnetic flux density magnitude as functions of $\omega/\omega_c = q^2$ at radial locations of 0 (cylindrical axis), $0.2R$, $0.4R$, $0.6R$, $0.8R$, and $0.9R$ (distance from the axis increases from red to blue – the direction of the arrow). (For interpretation of the references to color in this figure legend, the reader is referred to the web version of this article.)

attenuation depends on the nature and requirements of a given application. Selecting 10% attenuation as an example, the forcing frequency should be kept below about 0.63 times the cut-off frequency. If this condition cannot be met, the cut-off frequency should be increased by altering the bias condition, changing the material, or decreasing the rod's radius. If this does not suffice, the material can be laminated to reduce the effect of eddy currents.

The real and imaginary parts of the eddy current factor for mechanically induced magnetic diffusion are presented in Fig. 5.

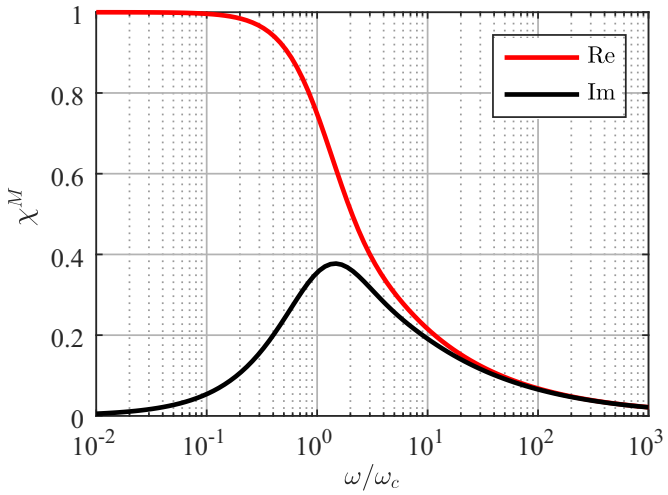

Fig. 5. Real and imaginary parts of χ^M, the eddy current factor for mechanically induced magnetic diffusion, as a function of $\omega/\omega_c = q^2$.

Since this plot is general, it can be used with (58) to directly calculate a complex-valued magnetoelastic coupling coefficient for incorporating mechanically induced magnetic diffusion effects in any magnetoelastic material.

7. Conclusions

This paper considered the radial dependence of the magnetic field inside cylindrical magnetoelastic materials that results from eddy currents that are induced by the application of a harmonic, axial mechanical input; this effect, which is particularly pronounced in magnetostrictive materials and ferromagnetic shape memory alloys, was termed mechanically induced magnetic diffusion to distinguish it from the conventional magnetic field-induced magnetic diffusion. The PDE governing radial diffusion was derived from the general magnetic diffusion equation by considering the symmetry of the problem and assuming linear constitutive behavior, uniform stress, and negligible demagnetizing fields. Analytical time- and frequency-domain solutions were derived using the method of eigenfunction expansions. By non-dimensionalizing the dynamic magnetic field and deriving a penetration (skin) depth δ^M and cut-off frequency ω_c^M for mechanically induced diffusion, the solutions were non-dimensionalized (i.e., made applicable to all magnetoelastic materials). The skin depth and the cut-off frequency are

$$\delta^M \approx 2.0831(\mu\sigma\omega)^{-1/2} = 2.0831\delta^H \tag{62}$$

and

$$\omega_c^M \approx 4.3393\left(\mu\sigma R^2\right)^{-1} = 4.3393\omega_c^H, \tag{63}$$

respectively, where δ^H and ω_c^H are the skin depth and the cut-off frequency for field-induced diffusion in cylinders, respectively. By defining an effective internal magnetic field as the average field over the cylindrical rod's cross section, it was shown that the effects of mechanically-induced diffusion can be incorporated in 0D constitutive models through the use of a complex-valued magnetoelastic coupling coefficient and Young's modulus.

The non-dimensionalized solutions were plotted to illustrate the response of these materials to mechanically induced diffusion. The spatial distribution of the magnitude of the non-dimensionalized dynamic field was given for a wide range of skin depths. For forcing frequencies below about 5 times the cut-off frequency (or equivalently, for rods with radii less than about 2.2 times the skin depth), the dynamic, internal magnetic field increases monotonically from zero at the rod's surface to a maximum at its axis. The internal field at the axis also phase lags behind the field closer to the surface. Up to about the cut-off frequency, the magnitude of the steady-state, dynamic field increases in proportion to $f^{1.0}$. As forcing frequency increases above that range, the magnitude overshoots its high frequency limit, peaks, then decreases to its high frequency limit, at which point the dynamic magnetic flux becomes zero and further increases in forcing frequency have no effect. The magnitude response of the dynamic magnetic flux was also presented. Given a maximum desired attenuation of the magnetic flux density, this magnitude response can be used to define design criteria for many applications, including dynamic sensors, energy harvesters, vibration dampers, and tunable stiffness devices. For example, for a maximum attenuation of 10%, the forcing frequency should be kept below about 0.63 times the cut-off frequency. The normalized real and the imaginary part of the eddy current factor were plotted as a function of the normalized forcing frequency. Given a material of known properties, the complex-valued magnetoelastic coupling coefficient can be directly calculated from this plot.

Acknowledgments

This work was supported by the NASA Aeronautics Scholarship Program (Grant # NNX14AE24H). Additional support was provided by the member organizations of the Smart Vehicle Concepts Center (http://www.SmartVehicleCenter.org), a National Science Foundation Industry/University Cooperative Research Center.

References

[1] C.T.A. Johnk, Engineering Electromagnetic Fields and Waves, John Wiley & Sons, Inc, New York, 1988.
[2] L. Lefebvre, S. Pelletier, C. Gelinas, Effect of electrical resistivity on core losses in soft magnetic iron powder materials, J. Magn. Magn. Mater. 176 (2) (1997) L93–L96, http://dx.doi.org/10.1016/S0304-8853(97)01006-8.
[3] J. Szczygłowski, Influence of eddy currents on magnetic hysteresis loops in soft magnetic materials, J. Magn. Magn. Mater. 223 (1) (2001) 97–102, http://dx.doi.org/10.1016/S0304-8853(00)00584-9.
[4] L. Kvarnsjö, G. Engdahl, Examination of the interaction between eddy currents and magnetoelasticity in Terfenol-D, J. Appl. Phys. 69 (8) (1991) 5783–5785, http://dx.doi.org/10.1063/1.347875.
[5] D. Kendall, A.R. Piercy, Comparison of the dynamic magnetomechanical properties of $Tb_{0.27}Dy_{0.73}Fe_2$ and $Tb_{0.30}Dy_{0.70}Fe_2$, J. Appl. Phys. 76 (10) (1994) 7148–7150, http://dx.doi.org/10.1063/1.357991.
[6] P. Rasilo, D. Singh, A. Belahcen, A. Arkkio, Iron losses, magnetoelasticity and magnetostriction in ferromagnetic steel laminations, IEEE Trans. Magn. 49 (5) (2013) 2041–2044, http://dx.doi.org/10.1109/TMAG.2013.2242857.
[7] N.N. Sarawate, M.J. Dapino, Dynamic sensing behavior of ferromagnetic shape memory Ni–Mn–Ga, Smart Mater. Struct. 18 (10) (2009) 104014, http://dx.doi.org/10.1088/0964-1726/18/10/104014.
[8] M.J. Dapino, P.G. Evans, Constitutive modeling for design and control of magnetostrictive Galfenol devices, Adv. Sci. Technol. 54 (2009) 13–18, http://dx.doi.org/10.4028/www.scientific.net/AST.54.13.
[9] D. Davino, A. Giustiniani, C. Visone, Effects of hysteresis and eddy currents in magnetostrictive harvesting devices, Phys. B: Condens. Matter 407 (9) (2012) 1433–1437, http://dx.doi.org/10.1016/j.physb.2011.07.038.
[10] D. Davino, A. Giustiniani, C. Visone, W. Zamboni, Stress-induced eddy currents in magnetostrictive energy harvesting devices, IEEE Trans. Magn. 48 (1) (2012) 18–25, http://dx.doi.org/10.1109/TMAG.2011.2162744.
[11] X. Zhao, D. Lord, Application of the Villari effect to electric power harvesting, J. Appl. Phys. 99 (8) (2006) 08M703, http://dx.doi.org/10.1063/1.2165133.
[12] N.H. Asmar, Partial differential equations and boundary value problems with Fourier series and boundary value problems, 2nd ed., Pearson Prentice-Hall, Upper Saddle River, NJ, 2000.
[13] G. Engdahl, Handbook of Giant Magnetostrictive Materials, Academic Press, San Diego, CA, 2000.